Proceedings of the 28th IEEE
EMBS Annual International Conference
New York City, USA, Aug 30-Sept 3, 2006

Parametric Reconstruction Method in Optical Tomograhy

Xuejun Gu, Kui Ren, James Masciotti and Andreas H. Hielscher

Abstract— **Optical tomography consists of reconstructing the spatial of a medium's optical properties from measurements of transmitted light on the boundary of the medium. Mathematically this problem amounts to parameter identification for the radiative transport equation (ERT) or diffusion approximation (DA). However, this type of boundary-value problem is highly ill-posed and the image reconstruction process is often unstable and non-unique. To overcome this problem, we present a parametric inverse method that considerably reduces the number of variables being reconstructed. In this way the amount of measured data is equal or larger than the number of unknowns. Using synthetic data, we show examples that demonstrate how this approach leads to improvements in imaging quality.**

I. INTRODUCTION

Large strides have been made over the last 10 years towards optical tomographic imaging (OTI)of biological tissues [1]. With the emergence of the appropriate light detection technology [2], [3], [4] and suitable image reconstruction codes [5], the field has increasingly focused on clinical and preclinical applications.While first clinically relevant applications have emerged, there still remain significant challenges with respect to the low spatial resolution of the images and the non-uniqueness (ill-posedness) of the image reconstruction problem.[5].

One of the reasons for these problems is that usually the number of unknown parameters to be reconstructed by far exceed the number of measurement data available. Therefore the number of "knowns" is substantially smaller than the number of unknowns in the resulting system of algebraic equations. To overcome this problem researchers have suggested multi-spectral method – using several wavelengths [6] or multi-frequency measurement system [7]. In both these methods the number of measurement data ("knowns") is increased. In another direction, researchers have looked for ways to reduce the number of unknowns by combining different imaging modalities, such as magnetic resonance imaging (MRI) and OTI [8] or ultrasound and OTI [9]. In these cases, MRI or ultrasound provide the prior structural information for optical imaging.

In this paper, we introduce a novel numerical algorithm that decrease the number of unknowns in the image reconstruction process. The spatial varying optical-property map is decomposed into space-frequency spectra using a discrete Fourier Transform (DFT). Instead of reconstructing each pixel in an image independently, we reconstruct only the spectral moments that represent the majority of the information contained in an image. A simple calculations demonstrates how this approach leads to a reduction of the number of unknowns. For example, in optical tomography, if we discretize a 2×2 cm 2D domain to 40×40 and only reconstruct absorption coefficients, there be will 1600 unknowns. In contrast, using the suggested parametric reconstruction method to reconstruct 10 moments will yield only 400 unknown variables.

In this paper, we employ the frequency-domain equation of radiative transport (ERT) as a model of light propagation in tissue. However, it should be noted that the parametric reconstruction method is also suitable for a diffusion-theory-based model. In section 2, we briefly review the pertinent aspects of the ERT and related non-parametric (pixel) reconstruction scheme. The parametric reconstruction method using DFT will be presented in section 3. To illustrate the performance of these codes, we show some numerical results in section 4. The paper closes with a discussion and an outlook on future work.

II. RECONSTRUCTION METHOD IN OPTICAL TOMOGRAPHY

A. Forward Problem

The forward problem of the frequency-domain ERT has already been detailed [10]. The frequency-domain ERT that describes the photon density in the phase space, i.e ., as a function of position $\mathbf{x} \in \mathcal{D} \subset \mathbb{R}^n$ and direction $\boldsymbol{\theta} \in S^{n-1}$ (unit sphere of $\mathbb{R}^n$), is given by

$$\begin{array}{rcll} \left(-\frac{i\omega}{v} + \boldsymbol{\theta}\cdot\nabla + \mu_t(\mathbf{x})\right)\psi(\mathbf{x},\boldsymbol{\theta}) & & & \\ -\mu_s(\mathbf{x})\int_{s^{n-1}} k(\boldsymbol{\theta}\cdot\boldsymbol{\theta}')\psi(\mathbf{x},\boldsymbol{\theta}')\,d\boldsymbol{\theta}' & = & 0 & \text{in } \mathcal{D}\times S^{n-1} \\ \psi(\mathbf{x},\boldsymbol{\theta}) & = & q(\mathbf{x},\boldsymbol{\theta}) & \text{on } \Gamma_-. \end{array} \quad (1)$$

where $i = \sqrt{-1}$, v is the speed of light in the medium, and ω is the source modulation frequency. The parameter $\mu_t = \mu_a + \mu_s$, with μ_a and μ_s being the absorption and scattering coefficient, respectively. $\psi(\mathbf{x},\boldsymbol{\theta})$ is the radiance at position $\mathbf{x}$ ($\mathbf{x} \in D$) traveling in direction $\boldsymbol{\theta}$ with the unit of $Wm^{-2}sr^{-1}$. Note that $\psi(\mathbf{x},\boldsymbol{\theta})$ is frequency-dependent. $q(\mathbf{x},\boldsymbol{\theta})$ is a source with the unit of $Wm^{-3}sr^{-1}$ defined on the boundary set:

$$\Gamma\pm = \{(\mathbf{x},\boldsymbol{\theta}) \in \partial\mathcal{D}\times S^{n-1} \text{ s.t. } \pm\boldsymbol{\theta}\cdot\boldsymbol{\nu}(\mathbf{x})\},$$

The "collision" kernel $k(\boldsymbol{\theta}\cdot\boldsymbol{\theta}')$, which describes the probability that photons traveling in direction $\boldsymbol{\theta}'$ scatter into

Xuejun Gu is with the Department of Biomedical Engineering, Columbia University, NY 10027, xg2108@columbia.edu

Kui Ren is with the Department of Applied Physics and Applied Mathmatics, Columbia University, NY 10027, kr2002@columbia.edu

James Masciotti is with the Department of Biomedical Engineering, Columbia University, NY 10027, jmm2014@columbia.edu

Andreas H.Hielscher is with the Departments of Biomedical Engineering and Radiology, Columbia University, NY 10027, ahh2004@columbia.edu

direction $\boldsymbol{\theta}$, is a positive function independent of $\mathbf{x}$ and satisfies the normalization condition:

$$\int_{S^{n-1}} k(\boldsymbol{\theta}\cdot\boldsymbol{\theta}')d\boldsymbol{\theta}' = 1. \quad (2)$$

The scattering kernel for light propagation in tissues is chosen here as the Henyey-Greenstein phase function [11].

Solving the forward problem (1), will give the quantity of radiance. However, in optical tomography experiments the quantity that one measures is the outgoing flux. This flux can be expressed as

$$J(\mathbf{x}_d) = \int_{\Gamma_+} \boldsymbol{\theta}_d \cdot \boldsymbol{\nu}\psi(\mathbf{x}_d, \boldsymbol{\theta}_d)d\boldsymbol{\theta}_d, \quad (3)$$

where $\mathbf{x}_d$ is the position of detector and $J(\mathbf{x}_d)$ is a complex functional of the optical paramters μ_a and μ_s.

With the combination of the discrete ordinates method [12] for the angular variable and a finite-volume discretization method for the space variable ,the ERT can be converted to the following algebraic equation:

$$\mathbf{A}\boldsymbol{\Psi} = \mathbf{S}\boldsymbol{\Psi} + \mathbf{Q}. \quad (4)$$

B. Inverse problem with non-parametric methods

Using the ERT forward model, we can predict how the lights propagates inside the medium and what is measured on the boundary of the medium. In real optical tomography experiments only a limited number of boundary measurements are available. After discretizing (1) with a reasonable mesh, one usually has a very underdetermined system with which to reconstruct the optical property map. Classically, a least square problem is formulated and a regularization term is added to compensate for this underdetermination. Numerically, this requires the minimization of the following objective function:

$$\min \mathcal{F}(\mu_a, \mu_s) = \frac{1}{2}\sum_{s=1}^{N_s}\sum_{d=1}^{N_d}\left(\mathcal{P}_{s,d}\boldsymbol{\Psi}_s - z_{s,d}\right)^2 + \frac{\alpha}{2}\sum_{\mathcal{C}=1} N \sum_{p=a,s}\left(\sum_{\kappa=x,y,z}(\mathcal{D}_\kappa^{\mathcal{C}}\mu_p)^2 + (\mu_p^{\mathcal{C}})^2\right). \quad (5)$$

Here $\mu_a = (\mu_a^1, \cdots, \mu_a^{\mathcal{C}}, \cdots, \mu_a^N)^T \in \mathbb{R}^{N\times 1}$ and $\mu_s = (\mu_s^1, \cdots, \mu_s^{\mathcal{C}}, \cdots, \mu_s^N)^T \in \mathbb{R}^{N\times 1}$ denote absorption and scattering coefficients respectively. $\mathcal{P}_{s,d}$ is the discretized form of the operator at detector position $x_{s,d}$ that integrates the outgoing flux over the boundary Γ_+ and $z_{s,d}$ donate the boundary measurement.

The second term is the regulariztion term and α is the regularization parameter. $\mathcal{D}_\kappa^{\mathcal{C}} \in \mathbb{R}$ denotes the discretized partial differential operator at cell C in $\kappa = (x, y, z)$ direction. We refer the interested reader to [13] for more details of the inverse algorithm of ERT.

III. Parametric Reconstruction Method

The algorithm described in the previous section treats each pixel of an image as an independent variable. Instead of treating each pixel as independent variable, we can also attempt to describe the image as a spatially varying function that is described by some functional that depends only on a small number of variables. The spatial Fourier transform can convert this image (spatial function) into a spatial frequency domain, where the image is decomposed into spatial Fourier spectra:

$$\mu_{p(=a,s)}(i,j) = \sum_{m=0}^{2M-1}\sum_{n=0}^{2N-1} A(m,n)cos(\frac{im\pi}{2M})cos(\frac{in\pi}{2N}) + B(m,n)cos(\frac{im\pi}{2M})sin(\frac{in\pi}{2N}) + C(m,n)sin(\frac{im\pi}{2M})cos(\frac{in\pi}{2N}) + D(m,n)sin(\frac{im\pi}{2M})sin(\frac{in\pi}{2N}), \quad (6)$$

where $\mu_{p(=a,s)}(i,j)$ is the absorption (scattering) coefficient with discretized coordinate (i, j). A(m, n), B(m, n), C(m, n), and D(m, n) are coefficients of Fourier moments. M and N are the total numbers of the moments.

The flowchart of image reconstruction with the parameteric reconstruction method is shown in Fig. 1.

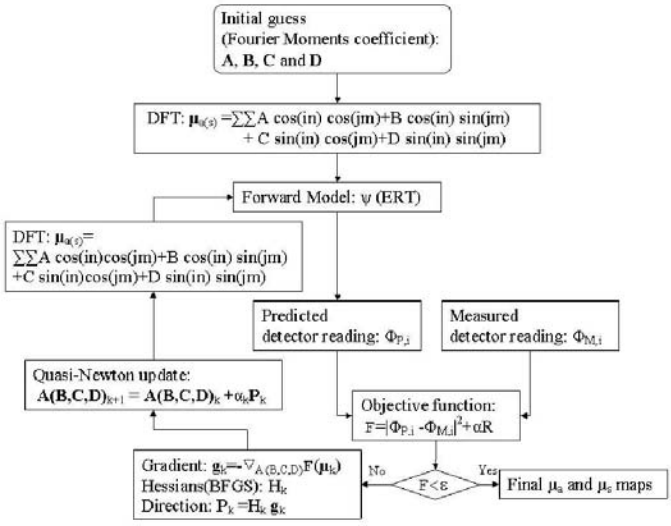

Fig. 1. Flow chart for the reconstruction of optical properties maps with parametric reconstruction method

IV. NUMERICAL EXAMPLES

We provide two numerical examples for illustrating the performance of the parameteric reconstruction method and compare the results of the parametric reconstruction scheme with the non-parametric pixel reconstruction method. The examples chosen here reconstruct only the absorption coefficient map with a fixed scattering coefficient map. Reconstructing the scattering maps can be implemented in the similar way. We focus on 2D domain reconstruction in this paper; however, the algorithm stated in section III can be easily extended to 3D.

A. Generating synthntic data

We consider a computational domain of size $2 \times 2\ cm^2$, given by $\mathcal{D} = [0,2] \times [0,2]$. This domain is disceitized into 80 cells of uniform size as:

$$\mathcal{D}_h = \{\mathbf{x}_{i,j} = (x_i, y_j),\ \mathrm{x}_i = i\Delta x,\ \mathrm{y}_i = i\Delta y,\ \mathrm{i,j} = 0,1,...,81\},$$

with $\Delta x = \Delta y = 0.025$. The direction space is discretized into 128 uniformly distributed directions with identical quadrature weight:

$$S^1_{\Delta\theta} = \{\theta_i : \theta_i = (i-1)\Delta\theta, i = 0, 1, \cdots, 80\},$$

where $\Delta\theta = 2\pi/80$. This discretization yields a total number of 512000 unknown if we only consider the reconstruction of one optical property. In both of the following cases, the measurement data are generated by forward computation rather than real experiments. Mimicing a real experimental setup, sources and detectors are placed around the boundary of a computational domain. Here, we put four sources (S4) located on the center of each boundary, and 156 detecteors (D156) evenly distributed around the domain. In each test, we generate $S4 \times D156 = 624$ measurement data, which is far fewer than the unknowns with the previous defined discretization. To test the parametric inverse algorithm, the snythntic data are generated with absorption spatial distribution function instead of momental distribution function.

B. Two testing Cases

In the first case, we put a single Gaussian distribution perturbation in the computational domain. The optical properties for this perturbation can be expressed as:

$$\begin{aligned} \mu_a(x,y) &= 0.1e^{-\frac{(x-1.4)^2+(y-1.0)^2}{0.045}} + 0.1\ cm^{-1} \\ \mu_s(x,y) &= 80\ cm^{-1}, \end{aligned} \tag{7}$$

The second case includes two absorption Gaussian distribution perturbations in the computational domain. The optical properties for this perturbation can be expressed as:

$$\begin{aligned} \mu_a(x,y) &= 0.1e^{-\frac{(x-1.4)^2+(y-1.0)^2}{0.025}} \\ &\quad +0.1e^{-\frac{(x-0.6)^2+(y-1.0)^2}{0.025}} + 0.1\ cm^{-1} \\ \mu_s(x,y) &= 80\ cm^{-1}, \end{aligned} \tag{8}$$

In both these two cases, the anisotropy factor g is 0.90 and the modulation frequency of the source is $\omega = 300MHz$.

Fig. 2 and 3 show the original absorption maps and reconstructed maps with pixel and parametric reconstruction method. Also shown are representative line plots of the cross-section absorption coefficient. Both of these two figures indicate that the parametric reconstructed image (Fig. 2(b) and 3(b)) achieve better geometrical shape than the pixel reconstructed image (Fig. 2(c) and 3(c)). Especially, in the case of two perturbations it is difficult to discern these two inhomogeneities using the non-parametric reconstruction method.

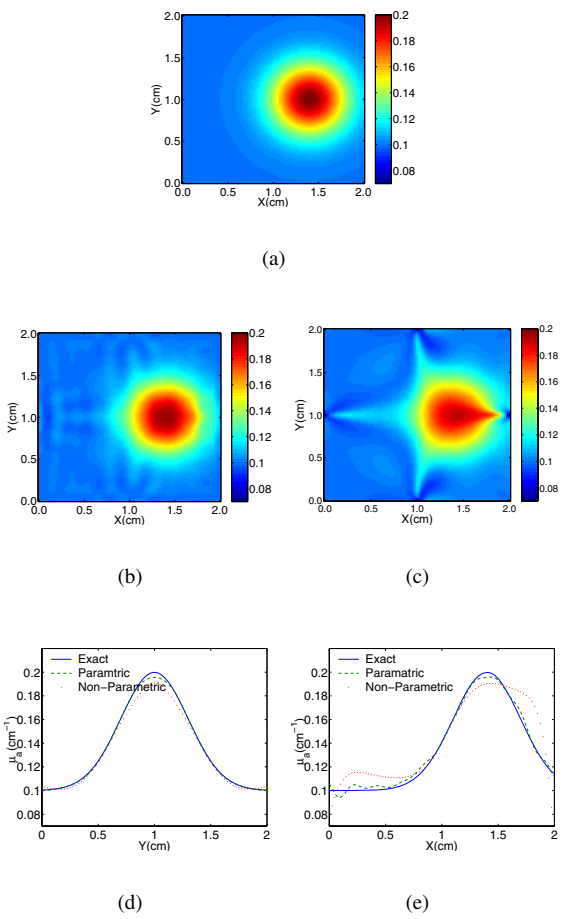

Fig. 2. Maps of reconstructed absorption coefficient $\mu_a[cm^{-1}]$ with single Gaussian distributed absorption perturbation; (a) exact setup absorption map; (b) parametric reconstructed absorption map; (c) pixel reconstructed absorption map; (d) cross sections of map (a) (solid line), (b)(dashed line) and (c) (dotted line) along the line x=1.4; (e) same as (d) except along the line y=0

C. Quality evaluation of reconstructed images

The quality of the reconstruction images are evaluated by two methods:

1) maximum error:

$$\varepsilon_{max} = \max \parallel M^r_{i,j} - M^o_{i,j} \parallel \ \mathrm{i,\ j} = 1,2,\cdots,80, \tag{9}$$

2) $\mathcal{L}^2$ norm error:

$$\varepsilon_{l^2} = \frac{\parallel M^r - M^o \parallel_{l^2}}{\parallel M^o \parallel_{l^2}} = \frac{\sqrt{\sum_{i=1}^{80}\sum_{j=1}^{80}(M^r_{i,j} - M^o_{i,j})^2}}{\sqrt{\sum_{i=1}^{80}\sum_{j=1}^{80}(M^r_{i,j})^2}}, \tag{10}$$

Here $M^o \in \mathbb{R}^{80\times80}(M^r \in \mathbb{R}^{80\times80})$ is an exact (reconstructed) image pixel values. A detailed comparsion of images quality is presented in Table I.

V. CONCLUSIONS AND FUTURE WORKS

We have formulated the inverse problem in optical tomography with a parametric method based on the frequency-domain ERT light propagation in biological tissue. The

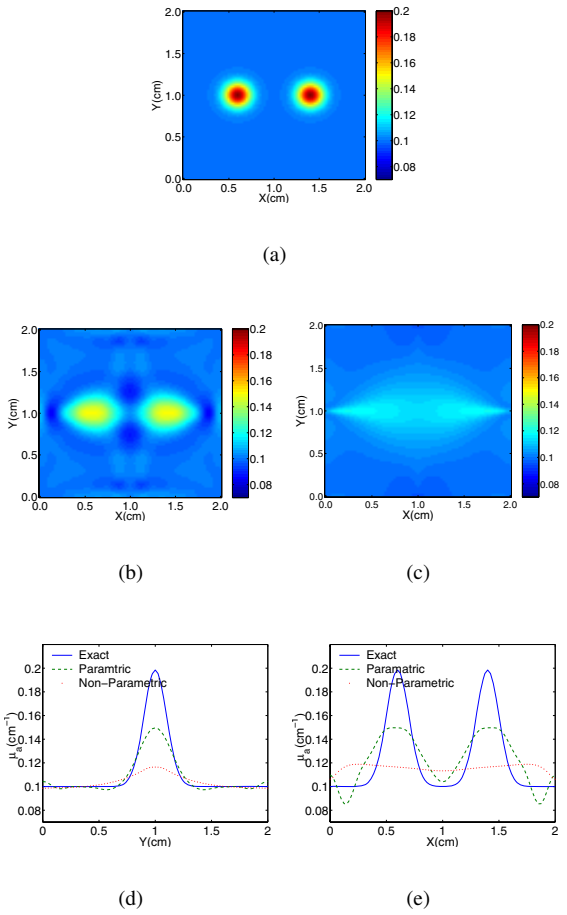

(a)

(b) (c)

(d) (e)

Fig. 3. Maps of reconstructed absorption coefficient $\mu_a[cm^{-1}]$ with two Gaussian distributed absorption perturbations; (a) exact setup absorption map; (b) parametric reconstructed absorption map; (c) pixel reconstructed absorption map; (d) cross sections of map (a) (solid line), (b)(dashed line) and (c) (dotted line) along the line x=1.4; (e) same as (d) except along the line y=0

TABLE I

ERRORS WITH DIFFERENT RECONSTRUCTION METHODS

Errors	One Gassuian Perturbation		Two Gassuian Perturbations	
	Parametric	Pixel	Parametric	Pixel
ε_{max}	0.0065	0.0425	0.0525	0.0919
ε_{l^2}	0.0085	0.0222	0.0488	0.082

advantages of using this method rely on a smooth distribution of optical properties in the tissue. We tested two cases with Gaussian-like perturbations. Compared to the non-parametric pixel reconstruction method, the parametric reconstruction method is a more stable inverse algorithm and yields more accurate images. Notably, for the case of two perturbations, the pixel reconstruction method failed to recover the original image, while the parametric succeeded in separating the two perturbations.

The method presented applies to optical tomography with ERT; however, this general Fourier decomposition method is also suitable for diffusion optical tomography, or even other inverse tomography methods, such as impedance or microwave tomography. As long as the reconstruction image is a smooth spatial function, this parametric reconstruction method can achieve better image quality comparing to pixel reconstruction.

With the parametric reconstruction method, a further understanding of our measurement data can be achieved. We can test different measurement geometries to extract information embedded in the measurement data, such as how many moments are available for the set measurement geometry. Extensive numerical reconstruction in practically experimental geometry will be performed in the future for choosing the best experimental setup.

VI. ACKNOWLEDGMENTS

We would like to thank Hilary Libka for many useful discussion and helpful suggestion concerning this manuscript. This work was supported in part by the National Institute of Biomedical Imaging and Bioengineering (NIBIB - grant R01 EB001900) and the National Institute of Arthritis and Musculoskeletal and Skin Diseases (NIAMS - grant 2R01-AR046255), which both are part of the National Institutes of Health (NIH).

REFERENCES

[1] B. Chance, R. Alfano, B. Tromberg, M. Tamura, and E. Sevick-Muraca, "Optical tomography and spectroscopy of tissue vi," in *SPIE-The International Society for Optical Engineering, Proceedings 5693*. Bellingham WA: SPIE, 2005.

[2] T. McBride, B. Pogue, S. Jiang, and U. Osterberg, "A parallel-detection frequency-domain near-infrared tomography system for hemoglobin imaging of the breast in vivo," *Rev. Sci. Instum.*, vol. 72, no. 3, pp. 1817–1824, 2001.

[3] C. Schmitz, H. Graber, Y.Pei, and R. Barbour, "Instrumentatin and calibration protocol for imaging dyanamic features in dense-scattering media by optical tomography," *Appl. Opt.*, vol. 39, no. 34, pp. 6466–6486, 2000.

[4] F. Schmidt, M. Fry, and E. Hillman, "A 32-channel time resolved instrument for medical optical tomography," *Rev. Sci. Instrum.*, vol. 71, no. 1, pp. 256–265, 2000.

[5] S. Arridge, "Optical tomography in medical imaging," *Inverse Problems*, vol. 15, no. 2, pp. R1–R93, 1999.

[6] A. Corlu, T. Durduran, R. Choe, M. Schweiger, E. M. C. Hillman, S. R. Arridge, and A. G. Yorh, "Uniqueness and wavelength optimization in continuous-wave multispectral diffuse optical tomography," *Opt. Lett.*, vol. 28, no. 23, pp. 2339–2341, 2003.

[7] G. Gulsen, B. Xiong, O. Birgul, and O. Nalcioglu, "Design and implementation of a multifrequency near-infrared diffuse optical tomography system," *J. BioMed. Opt.*, vol. 11, no. 1, p. 014020, 2006.

[8] D. Boas, A.M.Dale, and M. Franceschini, "Diffuse optical imaging of brain activation:approches to optimizing image sensitivity, resolution, and accuracy," *NeroImage*, vol. 23, no. S1, pp. S275–288, 2004.

[9] M. Huang and Q. Zhu, "A dual-mesh optical tomography reconstruction method with depth correction usign a priori ultrasound information," *Appl. Opt.*, vol. 43, no. 8, pp. 1654–1662, 2004.

[10] K. Ren, G. Abdoulaev, G. Bal, and A. Hielscher, "Algorithm for solving the equation of radiative transfer in the frequency domain," *Opt. Lett.*, vol. 29, no. 6, pp. 578–580, 2004.

[11] L. Henyey and J. Greenstein, "diffuse radiation in the galaxy," *Astrophysi. J.*, vol. 90, no. 16, pp. 70–83, 1941.

[12] E. E. Lewis and W. F. Miller, *Computational Methods of Neutron Transport*, 2nd ed. La Grange Park, IL: American Nuclear Society, 1993.

[13] K. Ren, G. Bal, and A. Hielscher, "Frequency domain optical tomography with the equation of radiative transfer," *Accepted for publication in SIAM Journal of Scientific Computing*, 2006.